AIAA JOURNAL
Vol. 41, No. 12, December 2003

Oil-Film Interferometry Skin-Friction Measurement Under White Light

Jean-Michel Desse*
ONERA, 59045 Lille Cedex, France

The interference fringes obtained under white light by a thin oil film were used to measure distribution of the skin-friction coefficient on a flat plate. The model placed in a subsonic flow was illuminated by a 500-W xenon white light source. The film height and variation over time were measured by analyzing the fringe colors that were similar to those of Newton's tints. The use of color shows that very high accuracy can be achieved for interferogram analysis using a numerical model of the phenomenon based on a nonconstant stress assumption. Experimental data were compared with those obtained by solving the simplified Navier–Stokes equations and with the solutions supplied by a boundary-layer code. Experiments showed that the white light interferometry technique was well suited to determine the transition region and that the stress levels varying from a few pascals up to around a hundred pascals were measured with an accuracy of a few percent. The main sources of error were identified, and their effects were quantified.

Nomenclature

a_0	=	amplitude of the incident wave
C_f	=	friction coefficient
C_v	=	interference fringe visibility coefficient
e	=	boundary-layer thickness
H	=	boundary-layer shape parameter
h	=	oil-film height
M	=	Mach number
n	=	refraction index of the medium
P	=	pressure
Re_x	=	Reynolds number
R_1, R_2	=	reflection coefficients on air–oil and oil–Mylar® interfaces, respectively
T	=	temperature
T_1, T_2	=	transmission coefficients on air–oil and oil–Mylar interfaces, respectively
t	=	time
t_0	=	wind tunnel starting time
U, V, W	=	velocity components on the x, y, and z axes
x'	=	oil abscissa
x'_0	=	oil leading-edge origin
δ	=	optical path difference
δ^*	=	displacement thickness
θ	=	momentum thickness
θ_i	=	angle of incidence of the light source
μ	=	dynamic viscosity
ν	=	kinematic viscosity
ρ	=	density
τ_P	=	wall stress
0, x, y, z	=	Cartesian coordinate system whose origin is the model leading edge

Subscripts

0, a	=	for dynamic viscosity, relative to oil and air, respectively
0, ∞	=	for flow coefficients, values of the stagnation flow and of the freestream flow

Received 18 April 2002; revision received 13 December 2002; accepted for publication 23 December 2002. Copyright © 2003 by Jean-Michel Desse. Published by the American Institute of Aeronautics and Astronautics, Inc., with permission. Copies of this paper may be made for personal or internal use, on condition that the copier pay the $10.00 per-copy fee to the Copyright Clearance Center, Inc., 222 Rosewood Drive, Danvers, MA 01923; include the code 0001-1452/03 $10.00 in correspondence with the CCC.

*Engineer and Research Scientist, Applied Aerodynamics Department, 5, Boulevard Paul Painlevé; desse@imf-lille.fr.

I. Introduction

FRICTION drag represents nearly 50% of total drag for transport aircraft in cruise flight. Because of its importance, much work has been devoted in recent years to find a means of reducing drag, such as hybrid laminar flow control. During wind-tunnel testing, it is, therefore, necessary to be able to determine the local skin-friction coefficient with high accuracy. Research underway at ONERA to develope new methods to do so. There are currently several techniques for measuring the pressure on the surface of a model placed in a wind tunnel. They are based, for example, on the use of pressure sensitive paints or liquid crystals. (Attempts have been made to establish a relation between the paint degradation or the change of color of the liquid crystals and the surface pressure.) Another method, using thin oil films, consists of obtaining the wall stress directly from the measured oil-film height, thereby giving the skin-friction coefficient. This paper demonstrate the use of white light as an illumination source to measure the wall stress using oil film.

For about 25 years, much work has been undertaken, especially in the United States and the United Kingdom, to measure skin friction by depositing an oil film on the surface of the airfoil to be analyzed. The spread of the oil film and the variation of its height over time are observed by optical techniques, mainly based on interferometry. Identification of the interference fringes yields the oil-film height at a given time, from which is determined the shear stress on the airfoil in a given direction.

Note that the oil films to be measured are very thin (a few hundred nanometers to a few micrometers); thus, we felt it would be interesting to use white light rather than monochromatic interferometry because it is known that the former is very well suited to measuring very small optical path differences.

Skin-friction coefficient measurements were made on a flat plate model in a subsonic two-dimensional flow. The results are compared with those obtained by solving the simplified Navier–Stokes equations and with the solutions supplied by a boundary-layer code. Surveys of the boundary layer made with a flattened pitot probe at different abscissas also provide data for comparison.

The initial analysis used a model of the phenomenon based on the assumption that the wall stress is constant on the flat plate. An extension of this model is proposed to treat the regions where the stress is no longer constant. The results obtained show that it is possible to detect the transition on the wall with great accuracy.

II. Review of the Literature and Modeling of the Phenomenon

The initial work on the analysis of the movement of thin oil films subjected to an external airflow was conducted in 1976 and 1977 by Tanner and Blows[1] and Tanner.[2] The model of such a phenomenon can be written as an equation governing the oil-film flow on a surface caused by an external airflow. Note that the following equation includes external pressure and stress gradients:

$$\frac{\partial h}{\partial t} = \frac{1}{\mu_0}\left\{\frac{1}{3}\frac{\partial}{\partial x}\left(h^3\frac{\partial P}{\partial x}\right) - \frac{\mu_a}{2}\frac{\partial}{\partial x}\left[h^2\left(\frac{\partial U}{\partial y}\right)_{y=h}\right] + \frac{1}{3}\frac{\partial}{\partial z}\left(h^3\frac{\partial P}{\partial z}\right) - \frac{\mu_a}{2}\frac{\partial}{\partial z}\left[h^2\left(\frac{\partial W}{\partial y}\right)_{y=h}\right]\right\} \tag{1}$$

Squire proposed an equation derived from Eq. (1) by applying the conservation of the oil-film mass on the surface.[3] The oil-film flow was assumed to be slow and viscous, and its movement was described by the momentum equations (equations obtained from the Navier–Stokes equations by neglecting the convection terms). The boundary conditions are given by the flow external to the oil film, in particular, those obtained from the boundary-layer equations. At the air–oil interface, $y = h$, coupling between the air and oil flows requires the velocity and stress in the air and oil to be the same. It was hypothesized that the oil flow was two dimensional, incompressible, and slow moving. It was also assumed that the air boundary layer was much thicker than the oil film and that the pressure normal to the surface was constant. Note that the oil-film viscosity can be chosen such that the velocity of air at the edge of the boundary layer is always much higher than that of the oil. In this case, the ratio μ_a/μ_0 is small, and quantities $(\partial U/\partial y)_{y=h}$ and $(\partial W/\partial y)_{y=h}$ are approximately equal to τ_{xy}/μ_a and τ_{yz}/μ_a, respectively. In addition, in the case of conventional aerodynamic flows, the pressure gradient terms are often small and are second order in Eq. (1). Therefore, they can be neglected. If the shear stress is measured along the x axis, Eq. (1) simplifies to

$$\frac{\partial h}{\partial t} = -\frac{\partial}{\partial x}\left[\frac{h^2}{2}\tau_p\right] \tag{2}$$

A particular solution for this partial differential equation is

$$\tau_p = \mu_0 x'/ht \tag{3}$$

This particular solution corresponds to τ_p constant with x and at $t = 0$, $h = \infty$, where x' is measured from the upstream leading edge of the oil. To check linearized equation (3), Zilliac calculated the solution of Eq. (2) by finite differences.[4] He showed that after a short startup period (<10 s in his case), the analytic and finite difference solutions were in very good agreement. Application of Eq. (3) is the basis of the fringe imaging skin-friction technique developed by Monson and Mateer.[5] With this technique, the skin-friction coefficient is measured from a single interference fringe image obtained after stopping the wind tunnel. The blowing time and the fringe spacing are measured, and the stress is determined directly from these two parameters along with oil properties, computed from measured temperature. To decrease the sources of error, it is important for the wind-tunnel transient start up to be negligible compared to the air-on time. It can be seen that the oil-film thickness h varies as $1/t$ at a given x location, which means that, as the time increases, the oil-film thickness ratio becomes small, decreasing the measurement accuracy.

Application of the technique has already been demonstrated in large wind tunnels.[6] Very satisfactory results were obtained by Driver,[6] with a measurement accuracy of 5%. Some tests were even made in flight on full-scale aircraft by Drake and Kennelly.[7] Their measurements exhibited some dispersion, but they remained coherent and allowed localization of the boundary layer transition that develops on the wings of a Bonanza Beech F33C.

A second technique consists of recording interferograms at several instants during blowing. This is similar to the surface imaging skin-friction (SISF) technique.[8] This is the method we decided to test because it is more accurate. In fact, in our transonic facility, the wind-tunnel startup time is not negligible: it takes about 2 min to obtain the required Mach number. When Eq. (3) is examined, it can be seen that τ varies linearly with the product ht. If t_0 is the wind-tunnel starting time, product $h(t - t_0)$ must be constant when $t - t_0$ varies. For each interferogram, it is, therefore, sufficient to determine t_0 such that the product $h(t - t_0)$ is constant. Naughton and Brown[9] analyzed the errors of this technique and showed that the results were accurate within less than 5%. They also used the technique to measure skin-friction coefficients in complex flows.[10]

A extension of the model was proposed by Tanner and Blows[1] and Naughton and Brown[11,12] that assumed that τ_P was no longer constant with x. Equation (1) can be rewritten neglecting only the terms related to the pressure gradients and gravity:

$$\frac{\partial h}{\partial t} = \frac{1}{\mu_0}\left\{-\frac{1}{2}\frac{\partial}{\partial x}\left[\tau_x h^2\right] - \frac{1}{2}\frac{\partial}{\partial z}\left[\tau_z h^2\right]\right\} \tag{4}$$

When the flow is assumed to be two dimensional, the stress depends only on the x direction. Equation (4) can then be expanded between two computation steps, x_i and x_{i-1}, integrating the oil-film equation over time $t_1 - t_0$. Equation (4) is then written

$$(h_1 - h_0) + \frac{\partial}{\partial x}\left(\frac{\tau_x}{2\mu}\int_{t_0}^{t_1} h^2\,\mathrm{d}t\right) = 0 \tag{5}$$

The integral over time can be approximated by the product $h_0 h_1 \cdot \Delta t$ where h_0 and h_1 denote the oil-film thickness at times t_0 and t_1. Writing the spatial differences yields

$$(h_1 - h_0)_i + \frac{[(\tau_x/2\mu)h_0 h_1]_i - [(\tau_x/2\mu)h_0 h_1]_{i-1}}{(x_i - x_{i-1})} = 0 \tag{6}$$

It is then easy to determine the stress at abscissa i from that calculated at abscissa $(i - 1)$:

$$\tau_i = \frac{[(h_0 - h_1)_i/\Delta t + (\tau h_0 h_1/2\mu\Delta x)_{i-1}]}{(h_0 h_1/2\mu\Delta x)_i} \tag{7}$$

This more complicated method takes into account stress variations on the airfoil. Equation (7) requires knowing an initial value of τ_i. This value is given by assuming τ to be constant over a very small part of the model surface. It is obtained from Eq. (3).

A feasibility study of SISF was made in the light of this review of the literature, using a white light source (xenon, 500 W, high pressure) to demonstrate the ease of use and improved accuracy of the measurements.

III. Contribution of Color in the Oil-Film Thickness Measurement

In monochromatic interferometry, it is well known that the classical interference pattern is represented by a succession of dark and bright fringes. For two successive fringes, the optical path difference is equal to the wavelength of the laser source. When the light source is a continuous source (500-W xenon), the interference pattern is a colored fringe pattern in a sequence approximately matching Newton's color scale. This fringe's diagram allows the measurement of very small path differences because six or seven different colors define the interval 0–0.8 μm. However, when the path difference is greater than 3 or 4 μm, the colors can no longer be separated, and the larger path differences cannot be correctly measured.[13] On the other hand, the color contribution is interesting to determine directly the sign of the change in the oil-film thickness from the knowledge of the color in Newton's tints scale. Figure 1 shows an example: three different light sources are used to record the oil-film interference fringes in the vicinity of the boundary-layer transition region on a flat plate. The flow is from the left to the right, and the central part of the interferogram has been isolated to not take into account the

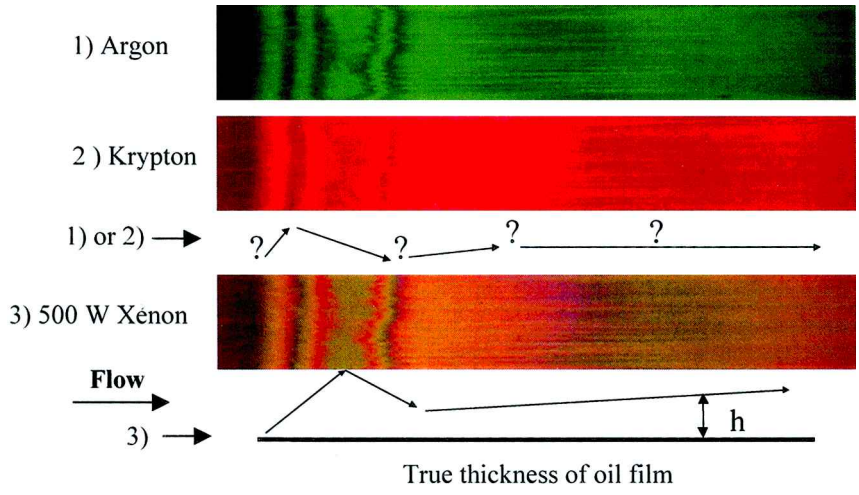

Fig. 1 Interference fringes obtained with three different light sources.

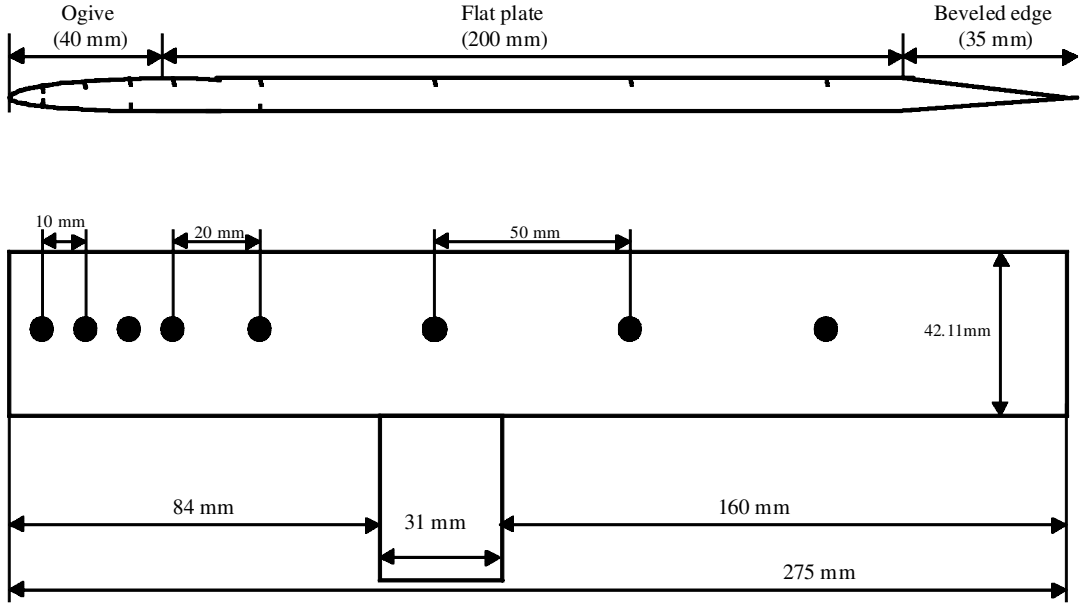

Fig. 2 Flat plate model.

test section lateral boundary layers. Interferograms 1 and 2 show interference fringes recorded with a green and a red line, respectively, issued from an argon and a krypton laser. The visualization of only dark and bright fringes does not allow the unambiguous determination of the evolution of the oil-film thickness. Interferogram 3 is obtained with a xenon light source, and the knowledge of Newton's tints scale allows the determination of the variation of the oil-film thickness without any doubt. Moreover, because no color is enclosed with two identical tints in Newton's scale, it is easy to detect the extrema of the oil-film thickness profile. This is important because the gradient changes of the oil-film profile are determined very easily. In interferogram 3 of Fig. 1, one can see that the pale green fringe is enclosed within two fringes having the same red color (first change in the oil-film thickness slope sign) and that the yellowish fringe is enclosed within two identically purplish-red colored fringes (second change of the slope sign). Analysis of the interferogram colors indicates that the oil-film thickness is increasing upstream of the location of the pale green color, then decreasing up to that of the yellowish color, and then increasing again downstream of it. This information is very difficult to obtain with a monochromatic light source. Also note that the oil-film thickness varies little downstream. Better sensitivity is obtained with a white light source because several fringes are visible downstream of the central part of the model. In monochromatic light (argon or krypton lasers), it is only possible to distinguish a variation of one fringe.

IV. Experimental Setup

Model and Instrumentation

The model is a flat plate 275 mm long, 42 mm wide, and 10 mm thick. Figure 2 shows that it consists of an ogive with a cubic profile to obtain a longer laminar boundary layer, a 200-mm flat section followed by a final 35-mm-long beveled edge. The model is equipped with eight pressure taps on the upper surface and four on the lower surface to adjust the angle of attack. It is held in the tunnel side walls. The tests were conducted in the ONERA–Lille transonic wind tunnel, the test section of which is two dimensional and 42 mm wide by 200 mm high. The freestream Mach number can be varied between 0.2 and 1, and two values have been chosen for the current experiment: 0.4 and 0.6. First, static pressures were measured on the model for both values of the Mach number, so that the angle of attack could be set at zero. Then, the boundary layer was surveyed at 60, 110, and 160 mm from the model leading edge. Oil drops were deposited on the model surface at different locations. The interference fringes photographed using a conventional film camera (f55 mm, at f11) at the rate of one frame per minute.

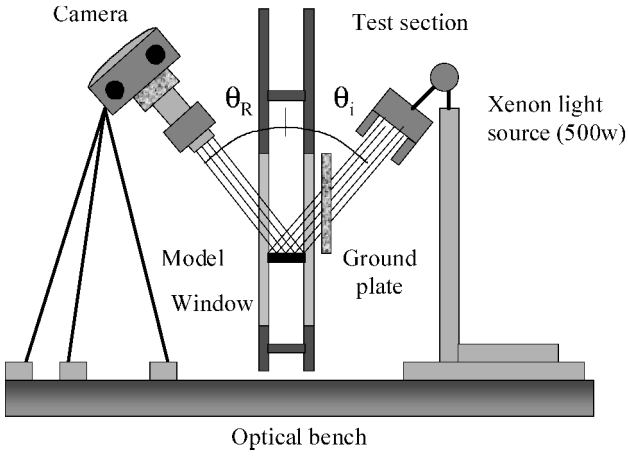

Fig. 3 Layout of the optical setup.

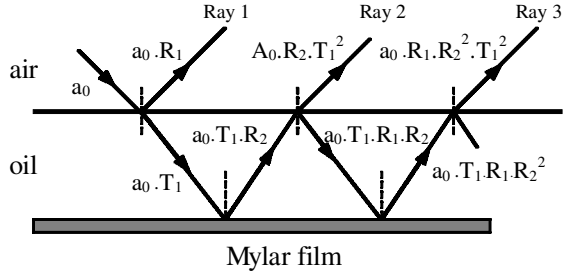

Fig. 4 Reflections and transmissions due to the different interfaces.

White Light Interferometry Setup

The white light interferometry system is very easy to set up. A 500-W xenon light source is placed on one side of the test section to illuminate the upper surface of the model at an angle of incidence θ_i. A camera placed on the other side of the test section at the same angle of incidence records the fringe images visualized on the model. Figure 3 shows an optical diagram of the setup in which a frosted glass is placed just opposite to the test section on the side of the incident beam. This greatly improves the quality of the fringe images because the frosted glass diffuses the light and turns the lamp into an extended source, which is the desired type of source for oil-film interferometry.

For each test, millimeter graph paper glued onto the model was photographed to calculate the enlargement on the x and y axes and to determine any distortions of the image. In all of the tests, a reference photograph was made at the time when the oil drop was deposited, to determine its abscissa before wind tunnel start up

Interference Considerations and Oil-Film Thickness Calculation

The light rays path is given in Fig. 4. The two reflected rays (denoted ray 1 and ray 2) have an optical path difference of δ, which depends on the thickness of the oil film, the refractive index, the incidence of illumination, and the wavelength. The oil-film thickness h vs δ is given by

$$h = \delta \Big/ 2\left(n_{\text{oil}}^2 - n_{\text{air}}^2 \sin^2 \theta_i\right)^{\frac{1}{2}} \tag{8}$$

When the denominator of Eq. (8) is denoted as $2 \cdot n_{\text{eq}}$, τ is written as

$$\tau_P = \frac{\mu_{\text{oil}} x' 2 \cdot n_{\text{eq}}}{\delta t} \tag{9}$$

When the viscosity ν of the oil is known, τ is determined by

$$\tau_P = 2\frac{\rho_{\text{oil}} \nu_{\text{oil}} x' n_{\text{eq}}}{\delta t} \tag{10}$$

Equation (10) is obtained by assuming that $\delta \tau_P / \delta x = 0$.

The contrast of the fringe images is defined by a visibility coefficient C_v defined from the maximum intensity $I_{\max}$ and minimum intensity $I_{\min}$ of the interference fringes:

$$C_v = \frac{I_{\max} - I_{\min}}{I_{\max} + I_{\min}} \tag{11}$$

When C_v is greater than 0.4, the fringe contrast is considered as acceptable. However, in fact, it is often low because the model material or coating does not have the ideal reflection coefficient to produce highly contrasted fringes. To overcome this drawback, a Mylar® film with a higher refractive index than the oil film is deposited on the model surface. The ideal refractive index for obtaining rays 1 and 2 of equal amplitude has been calculated from the reflection coefficients R_1 and R_2 and the transmission coefficients, $T_1 = 1 - R_1$ and $T_2 = 1 - R_2$, at the air–oil and oil–Mylar film interfaces. Because the refractive index of the silicone oils we used is around 1.4, the ideal refractive index of the film should be 1.982. Currently, a 20-μm-thick Mylar film is deposited on the model. Its refraction index is 1.67. The video camera used to digitize the interferograms has three internal filters with different spectral attenuation functions, so that different C_v are obtained on the three channels (0.63 on the red channel, 0.44 on the green one, and 0.33 on the blue one). These values provide fringe visibility and contrast for making satisfactory measurements.

We have also checked that the third ray appearing in Fig. 4 (ray 3) does not generate any spurious fringes. Its amplitude ($a_0 . T_1 . R_2 . R_1 . R_2 . T_1$) is computed at 0.00005%, which makes it absolutely negligible: There are no spurious fringes.

V. Interference Modeling

The model of the luminous interferences generated by a white light source (continuous spectrum) is described in Ref. 14. The principle of the model is based on spectral characterization of the entire interferometric system with the aim of creating the scale of experimental colors of the interferometer on a computer equipped with an image processing card when the optical path difference varies.

To do so, it is sufficient to make a spectrum analysis of the light source and use the optical transfer functions related to the interferometric setup and the three filters, red (R), green (G), and blue (B), of the camera used to digitize the interferograms. Several configurations can be used for recording and restoring the interferograms. Recording can be either directly digitized or done on a photographic film and digitized offline. For restoration, the image digitizing procedure requires illuminating the interferogram with the same light source as used for recording. In our case, we used the spectrum determined in earlier work for a 150-W high-pressure xenon light source using a monochromator coupled with a photomultiplier. For the present work, we used a 500-W halogen lamp.

To process the interferograms, the software allows the choice of an analysis window, the direction of the analysis (normal to the position of the interference fringes), and the interval between two analysis lines. For each analysis line, the color of each pixel is sought in the

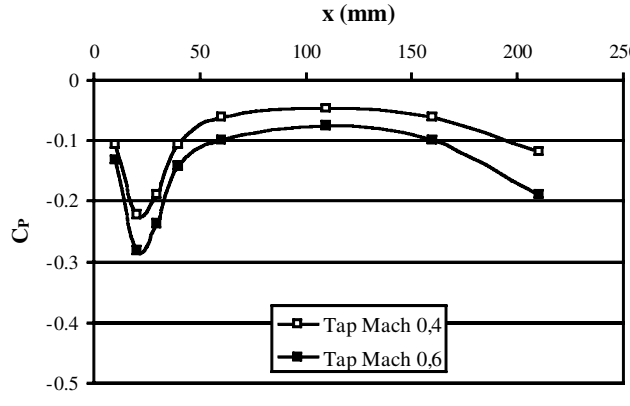

Fig. 5 C_P distribution on the model.

chart of experimental colors. When the color is found in the chart, the analyzed pixel is displayed on the monitor in this color. By use of the equivalence between the numerical and experimental charts, it is known that a color corresponds to an optical path difference δ. This path difference is displayed on the monitor for confirmation. A curve is obtained for each analyzed abscissa, which relates the optical path difference to the x abscissa. The search for δ is made with a resolution of 15 nm.

VI. Experimental Results

Pressure Distribution and Boundary Layer Surveys

Table 1 gives the locations of the pressure taps equipping the model in Cartesian x and y and curvilinear s coordinates, as well as the pressure coefficient measured at Mach 0.4 and 0.6. In Figure 5, coefficient pressure distribution has been drawn vs the x abscissa. At Mach 0.4 and 0.6, it can be observed that the pressure gradient is very weak for $60 < x < 150$ mm.

As mentioned, the boundary layer has been surveyed at three different abscissas, in each case with a pitot probe at the location of a pressure tap. The stagnation pressure was measured in the boundary layer using a probe whose orifice diameter was 0.23 mm. The surveys were difficult to make because of the small thickness of the boundary layer, especially at the most upstream location. The boundary-layer characteristics, that is, displacement thickness and momentum thickness, are obtained by integrating the probing profiles at Mach 0.4 and 0.6 and are given in Table 2. In addition, the friction coefficient can be calculated according to the logarithmic law for the shearing stress given by Squire and Young.[15] Finally, when our model is assimilated to an actual flat plate, we can estimate

Table 1 Pressure distribution on the model at Mach 0.4 and 0.6

	Tap number							
Characteristic	1	2	3	4	5	6	7	8
x, mm	10	20	30	40	60	110	160	210
y, mm	2.89	4.37	04.92	5	5	5	5	5
s, mm	10.42	20.53	30.55	40.55	60.55	110.55	160.55	210.55
C_P Mach 0.4	−0.107	−0.223	−0.188	−0.107	−0.061	−0.048	−0.061	−0.119
C_P Mach 0.6	−0.132	−0.283	−0.236	−0.142	−0.099	−0.076	−0.099	−0.189

Table 2 Boundary-layer characteristics and C_f deduced from Reynolds number

	x_{probing}, mm, Mach 0.4			x_{probing}, mm, Mach 0.6		
Characteristic	60	110	160	60	110	160
e, mm	0.76	1.59	2.26	0.95	1.64	2.28
$\delta,^*$ mm	0.163	0.226	0.368	0.160	0.267	0.351
θ, mm	0.085	0.152	0.242	0.089	0.175	0.236
$H = \delta^*/\theta$	1.93	1.48	1.52	1.81	1.53	1.48
C_f (Squire and Young[15])	0.00480	0.00417	0.00372	0.00430	0.00358	0.00338
$C_f = f(Rx)$	0.00420	0.00372	0.00345	0.00386	0.00342	0.00317

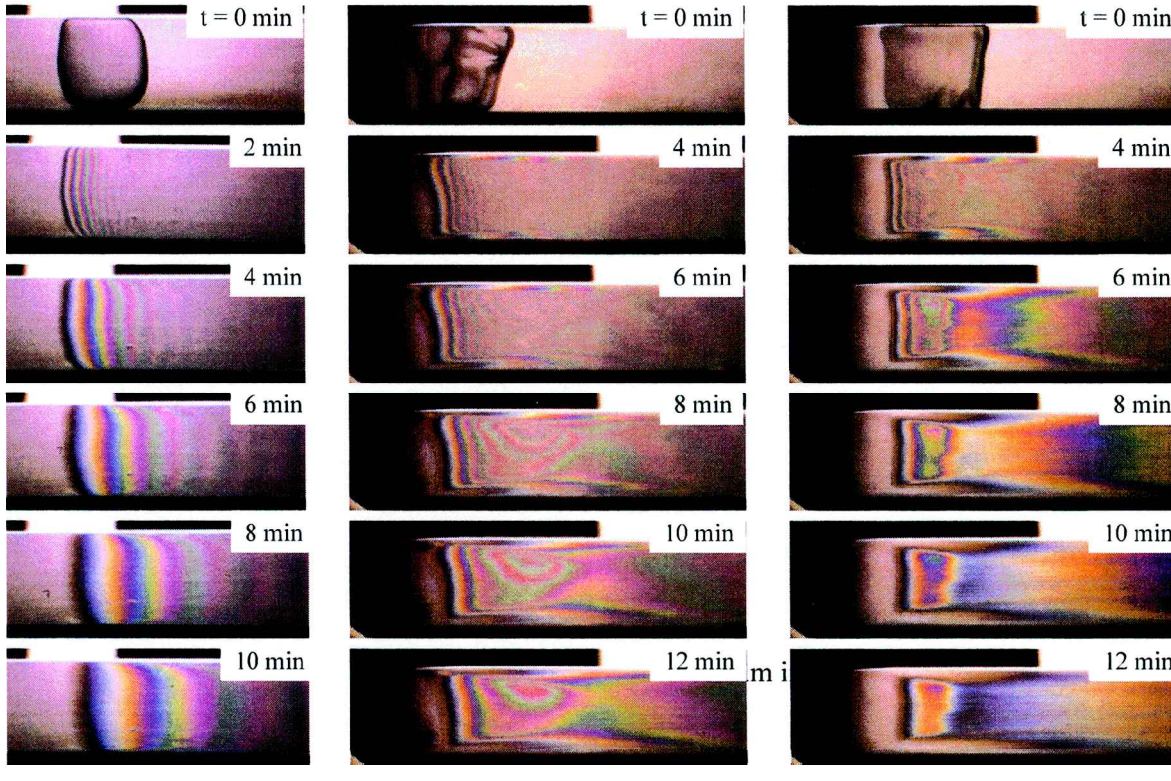

a) Mach 0.4, τ_P = const **b) Mach 0.4, $\tau_P = f(x)$** **c) Mach 0.6, $\tau_P = f(x)$**

Fig. 6 Variation with time of the oil film interferences.

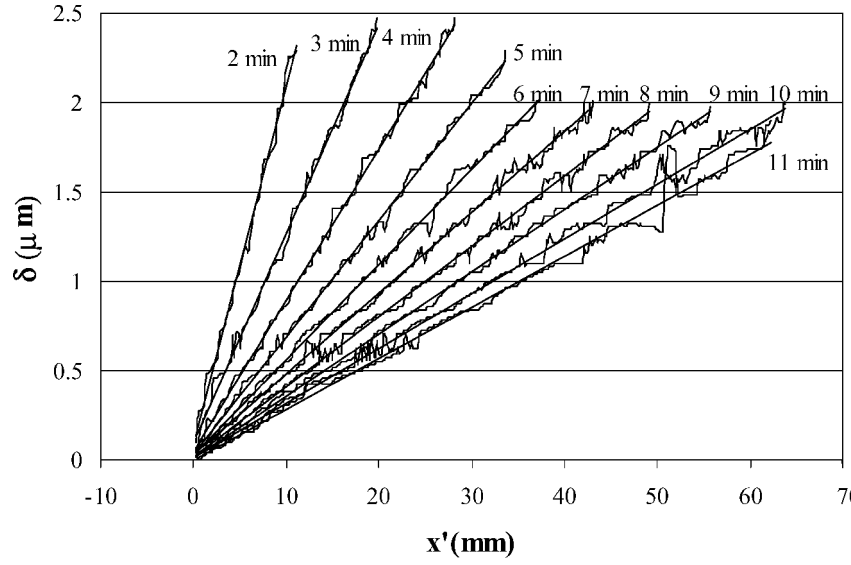

Fig. 7 Variation with time of the optical path differences.

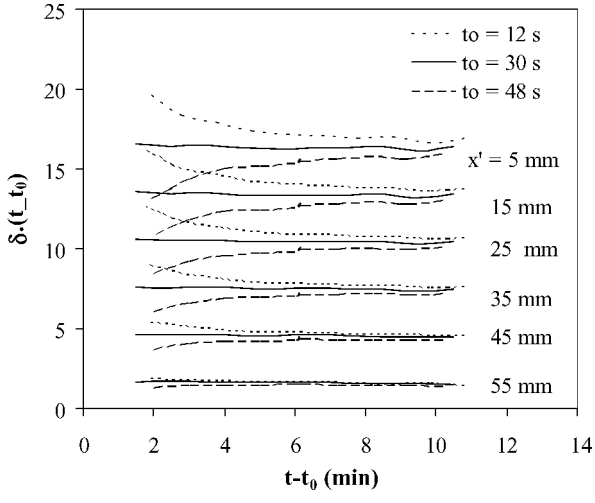

Fig. 8 Determination of wind-tunnel startup time t_0.

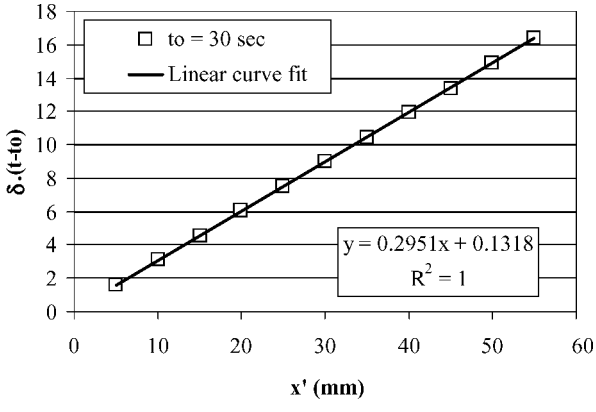

Fig. 9 Linear regression on product $\delta \cdot (t - t_0)$.

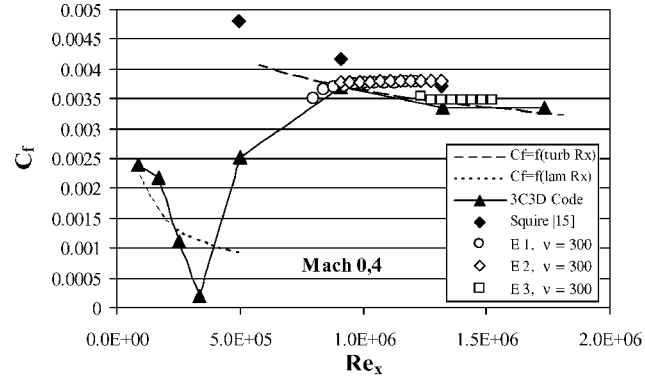

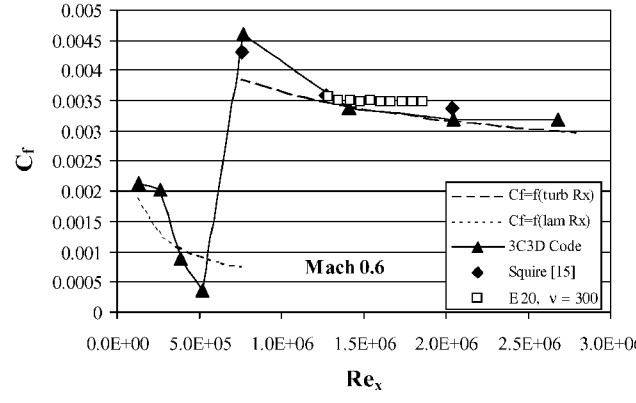

Fig. 10 Comparison between skin-friction coefficients assuming τ_p = const.

the friction coefficient according to the classical flat plate results of C_f vs Reynolds number (see Ref. 16). [$C_f = 0.664 \cdot (Re)^{-1/2}$ in laminar flow and $C_f = 0.058 \cdot (Re)^{-1/5}$ for a power law profile turbulent boundary layer.] At the probing abscissas (60, 110, and 160 mm), the boundary layer is turbulent for both test conditions, and the friction coefficients obtained are given in the last line of Table 2. In some of the figures that follow, the friction coefficient calculated from the Reynolds number is plotted in laminar state from the leading edge to 60 mm and in turbulent state from 60 mm to the trailing edge.

Results Obtained Assuming τ_P = Const

In the first tests, a drop of oil was deposited in a location where the pressure gradient was close to zero ($x = 110$ mm and $\nu = 300$ cSt), where the assumption of constant friction [$\tau_P(x) = \text{const}$] is verified. Figure 6a shows five interferograms recorded at 1-min time intervals. Because the photographs have been taken from the right-hand side of the tunnel, the flow is from right to left in all of the interferograms of Fig. 6. The oil film was deposited to have a roughly constant thickness over the full width of the test section. Time $t = 0$ is the wind-tunnel startup time. It can be seen that the fringe contrast is very good, which greatly facilitates analysis. The first five or six

orders of interference in white light can even very clearly be seen, after which the colors are no longer discernible.

In Fig. 6 the first photograph, it is easy to identify the origin of the oil drop. All of the results have been obtained by analyzing a single horizontal line. In the analysis, we measure the oil film thickness vs the distance x' downstream of the origin of the oil drop. The raw measurements of the optical path difference measured between interfering beams are plotted in Fig. 7 vs time. They vary almost linearly vs x', which allows a linear regression to be made for each time t, with correlation coefficients close to 1. The next step of the analysis consisted of evaluating the wind-tunnel startup time t_0. When Eq. (3) is examined, it can be seen that, for a given x', product $h \cdot t$ must be constant for each analysis time. Figure 8 shows the product $\delta \cdot (t - t_0)$ vs $t - t_0$ for values of t_0 equal to 12, 30, and 48 s for six different abscissas x'. It can be seen that for t_0 equal to 30 s, all of the curves are horizontal, which indicates the constancy of the product $h \cdot (t - t_0)$. The wind-tunnel starting time is, therefore, taken into account, and this procedure can be applied to any wind tunnel if the stress is constant on the airfoil. Note that a small error in t_0 is mainly perceptible during the first minutes of blowing. Therefore, it is necessary to find a tradeoff between the blowing time and the oil viscosity to measure t_0 accurately by the method shown in Fig. 8.

Figure 9 shows the variation of the product $\delta \cdot (t - t_0)$ vs x' for $t_0 = 30$ s. Linear regression in $\delta \cdot (t - t_0)$ indicates that the real abscissa of the oil drop origin is slightly different from the measured one. This particular point was also observed by Naughton and Brown, who attributed this offset to oil surface tension effects on the oil leading edge that were not taken into account in equations.[11] Here, the offset observed was 0.38 mm. We have chosen to use the measured drop origin for the analysis, not that obtained by the linear regression.

Figure 10 shows the variation of the skin-friction coefficient measured with the oil film for both Mach numbers. The values of 0.00375 for Mach 0.4 and 0.0035 for Mach 0.6 correspond to wall stresses of 39 and 75 Pa, respectively. In Figs. 10 we plotted C_f calculated from the Reynolds number for the part assumed to be laminar (front part of the plate up to 60 mm) and for the turbulent part (60 mm to the trailing edge). Computation results were also obtained from the ONERA 3C3D code by use of the pressure tap readings as inputs. C_f is calculated at the location of the taps and interpolated between them. The black symbols are the C_f values obtained from the boundary-layer surveys. The experimental values agree fairly well with either estimated value for the turbulent case. There are some discrepancies in the most downstream part, which may be attributed to the constant τ_P assumption, but even then, the overall levels are in good agreement.

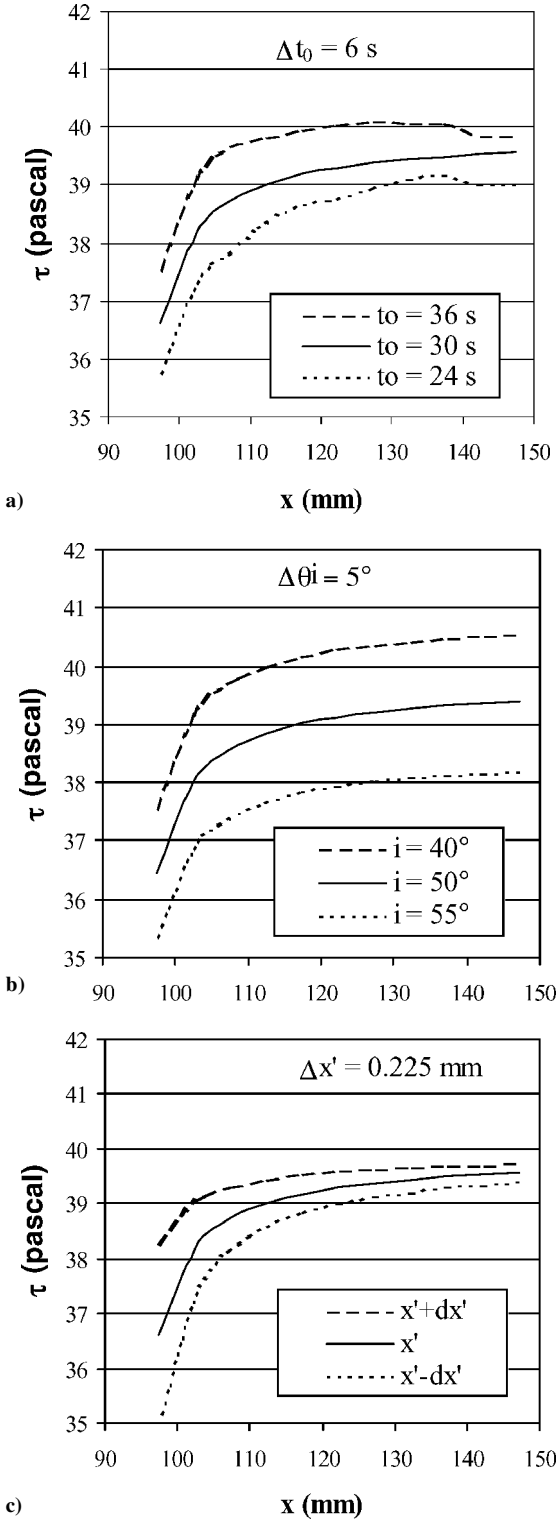

Fig. 11 Influence of experimental parameters.

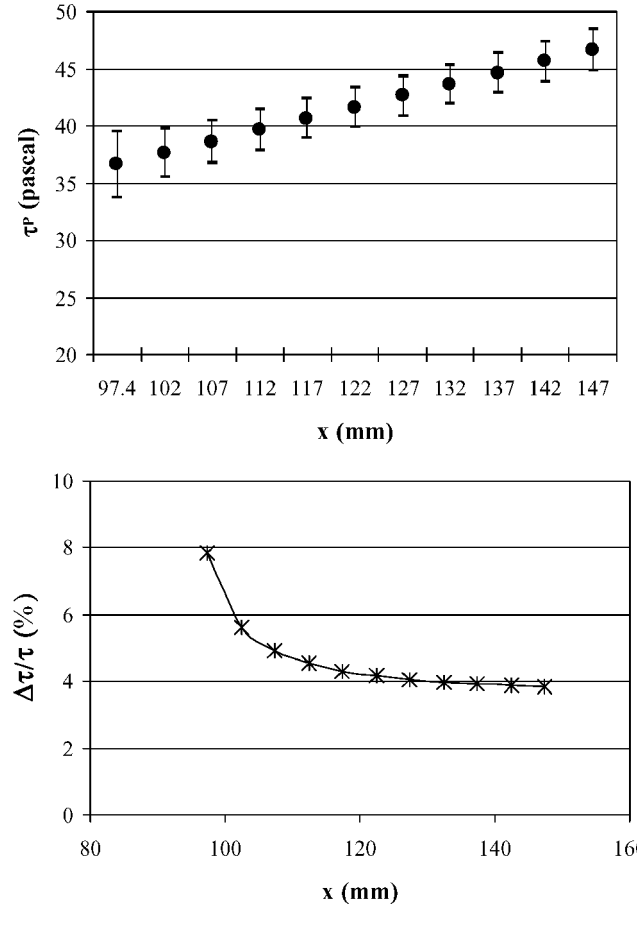

Fig. 12 Skin-friction coefficient measurement accuracy.

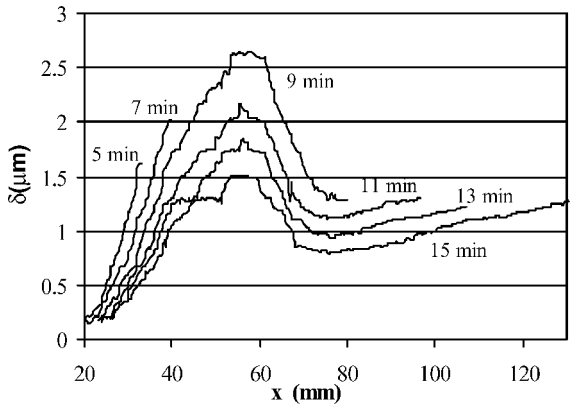

a)

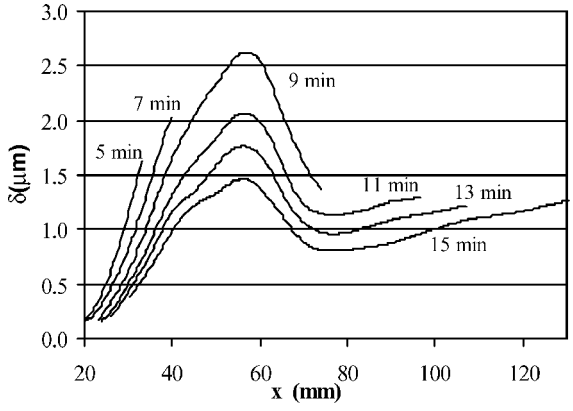

b)

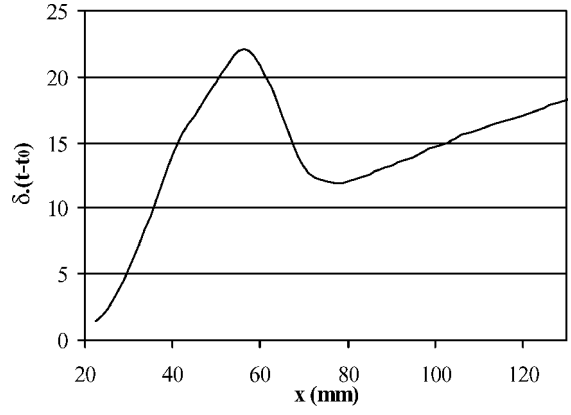

c)

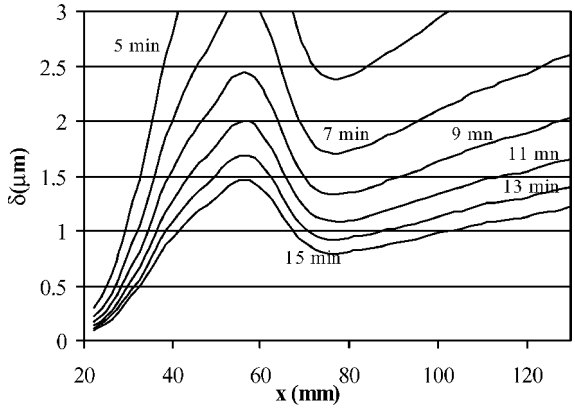

d)

Fig. 13 Mach 0.4: a) row measurements of δ, b) smoothed measurements of δ, c) average profile, and d) oil-film thickness recalculated from the average profile.

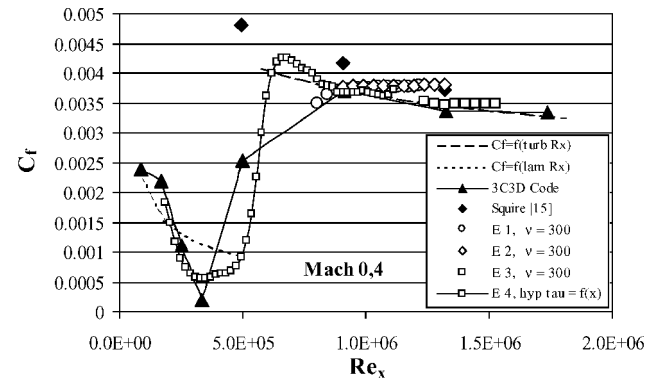

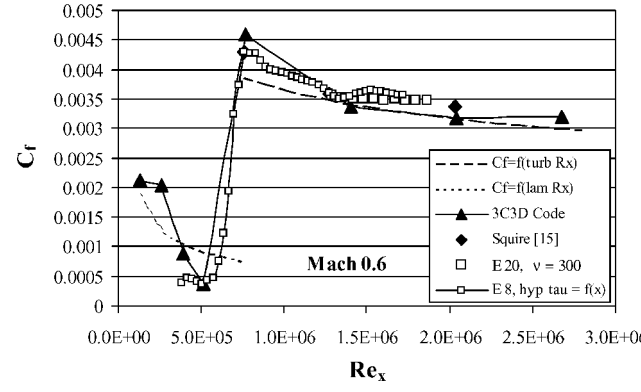

Fig. 14 Comparison between skin-friction coefficients assuming $\tau_p = f(x)$.

Influence of the Experimental Parameters

Figure 11 shows the influence of the three main experimental parameters: the wind-tunnel starting time t_0, the camera angle of incidence θ_i, and the oil drop origin x_0'. Figure 11a was obtained with an uncertainty of 6 s on t_0, Fig. 11b with an uncertainty of 5 deg for the camera angle, and Fig. 11c with an uncertainty of 0.225 mm of the location of the oil drop. For Figs. 11a and 11c, the uncertainty on the stress decreases very rapidly with the abscissa, whereas it is practically constant for Fig. 11b.

Note that the oil dynamic viscosity and density are manufacturer data. We measured the stagnation temperature during the tests, and the oil viscosity is corrected by taking into account the temperature in the boundary layer, which varies by a few tenths of a degree and has a weak influence on the oil viscosity, as has already been found by Zilliac[4] and Naughton and Brown,[9] who suggested to calibrate the specific oil sample and to carefully measure the temperature.

During the tests, we were able to evaluate the errors of these three parameters. We found 2 s for t_0, 2.5 deg for the angle of incidence, and 0.225 mm for the oil drop location. Figure 12 shows the variation of the measurement uncertainty and the relative variation of $\Delta\tau/\tau$ as a function of the abscissa x. When all other values are held constant (oil viscosity, temperature, etc.), it can be seen that the first measurement points have an accuracy of 8% and that the uncertainty is very rapidly cut in half, reaching 3.8%. This effect can be found on the first points of experimental values given in Fig. 10, where the values of the first points are slightly different from values of the following points. Therefore, it is important to measure correctly these three parameters.

Results Obtained Assuming $\tau_P = f(x)$

It seems interesting to deposit the oil upstream on the model to measure a larger area of the model. Several tests have been conducted depositing the oil at $x = 0$ or 30 or 40 mm. The viscosity was selected such that the blowing times were not too long and t_0 had little influence ($\nu = 100$ and 300 cSt). Figures 6b and 6c show six of the photographs taken for the two Mach numbers. This time, the interference fringes have an entirely different appearance. The oil-film

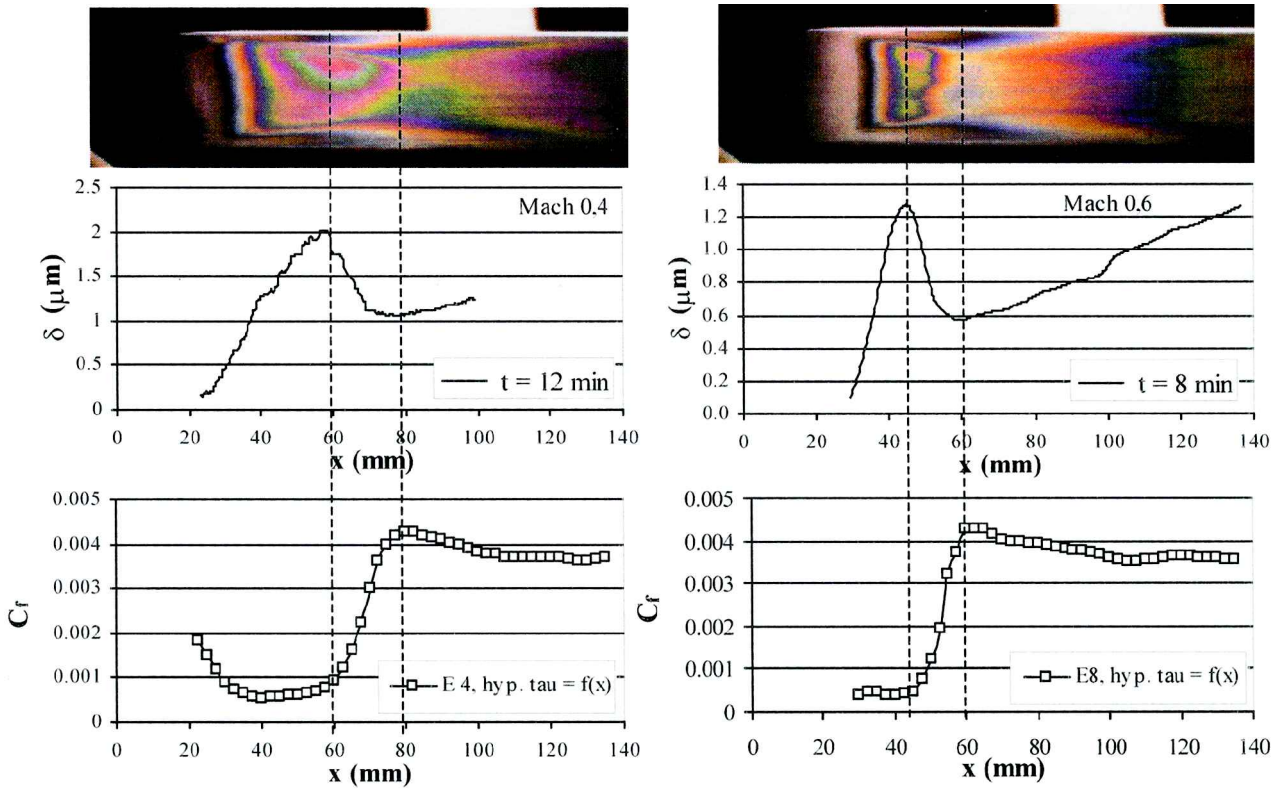

Fig. 15 Visualization of the transition location from interferograms.

thickness increases streamwise along the model, then decreases, and increases again in the rear part of the plate. This appearance is representative of boundary-layer transition. It can also be seen that the oil film thickness is not constant over the full width of the test section. Transition does not appear to be very two dimensional either.

All of these photographs (Figs. 6) were analyzed on a single horizontal line located at three-quarters of the span on the heel side of the model. The analysis of the raw optical path difference is given in Fig. 13a for Mach 0.4. The analysis method is the same for Mach 0.6. The recording times are 15 and 10 min, which minimizes the influence of t_0. Figure 13b shows the profiles obtained after smoothing the raw data. This yields very clean curves, which allow the wind-tunnel startup time t_0 to be determined by the procedure described earlier. However, this determination may not be very accurate because, when Eq. (7) is considered, the simple product $\delta \cdot t$ for a given x is not constant. The average value of $\delta \cdot (t - t_0)$ is calculated from the smoothed difference data for abscissas at 0.25-mm intervals. The averaged $\delta \cdot (t - t_0)$ curve is plotted in Fig. 13c vs reduced abscissa x. The oil-film thickness can be recalculated for any time interval $t - t_0$, as shown in Fig. 13d. Note that they are similar to the raw data curves.

The stress was obtained for each step from the stress obtained for the first computation point, assuming $\tau_P = \text{const}$ The results are plotted in Fig. 14 for the two Mach numbers. The variation of C_f shows that boundary-layer transition occurs between 50 and 80 mm for Mach 0.4 and between 40 and 60 mm for Mach 0.6. The stress level varies from 5 to 43 Pa then gradually drops to 37 Pa for the Mach 0.4 case. At Mach 0.6, levels vary from 8 to 92 Pa then drop to 75 Pa. At Mach 0.4, an increase of C_f at 80 mm is observed.

Finally, Fig. 15 shows two interferograms taken at Mach 0.4 and 0.6 at the instants 12 and 8 min. The corresponding oil-film thickness and the C_f distribution are shown just below the photographs. Two dotted lines are drawn at the abscissa determined by the change of sign of the oil-film thickness slope, which can be seen to coincide, in the interferograms, with the line surrounded by identically colored fringes and in the C_f graphs with the localization of the boundary-layer transition (important increase of the skin-friction coefficient). Qualitatively, the visualization of the interference fringes is sufficient to determine the transition zone of the boundary layer.

VII. Conclusions

The skin-friction coefficient on a flat plate model placed in a Mach 0.4 or Mach 0.6 flow has been measured using an oil film and white light interferometry. The model is coated with a Mylar film, which greatly improves the contrast of the observed interference fringes. The fringe images have been analyzed to determine the variation in time of the oil-film thickness on a very large area of the model. The phenomenon has been modeled with the assumption that the effects related to both pressure gradients and gravity are negligible. The results obtained from the oil-film thickness lead to the determination of transition on the airfoil and yield stress levels that agreed very well with those given by the boundary-layer code, with an accuracy of about 3%. The results are conclusive and validate the methodology.

The optical technique based on the use of a white light source is very easy to set up. Parameters such as the influence of the oil viscosity, pressure gradients, gravity, and curvature of the airfoil were not investigated.

The measurements made in white light show that they are limited to an oil-film thickness of a few micrometers. The technique can be extended by changing the light source and using a laser source consisting of three different wavelengths (R, G, and B). A trichromatic laser source would allow measurement of a much greater thickness, which would reduce the blowing time and increase the measurement accuracy, especially in the downstream part of the model. Finally, because of its possibilities and capability, this method should have many applications.

References

[1]Tanner, L. H., and Blows, L. G., "A Study of Motion of Oil Films on Surfaces in Air Flow with Application to the Measurement of Skin Friction," *Journal of Physics E: Scientific Instruments*, Vol. 9, No. 3, 1976, pp. 194–202.

[2]Tanner, L. H., "A Skin Friction Meter Using the Viscosity Balance Principle Suitable for Use of Flat Curved Metal Surfaces," *Journal of Physics E: Scientific Instruments*, Vol. 10, 1977, pp. 278–284.

[3]Squire, L. C., "The Motion of a Thin Oil Sheet Under the Steady Boundary Layer on a Body," *Journal of Fluid Mechanic*, Vol. 11, 1961, pp. 161–179.

[4]Zilliac, G. G., "Further Developments of the Fringe-Imaging Skin Friction Technique," NASA TM 1100425, Dec. 1996.

[5]Monson, D. J., and Mateer, G. G., "Boundary Layer Transition and Global Skin Friction Measurement with an Oil Fringe Imaging Technique," Society of Automotive Engineers, SAE Paper 932550, Sept. 1993.

[6]Driver, D., "Application of Oil Film Interferometry Skin Friction to Large Wind Tunnels," *Proceedings of the 81st AGARD Fluid Dynamics Pannel Meeting and Symposium*, CP 601, AGARD, 1997, pp. 25-1–25-10.

[7]Drake, A., and Kennelly, R. A., Jr., "Oil Film Interferometry for Skin Friction Measurement on an Aircraft in Flight," *8th International Symposium on Flow Visualization*, edited by G. M. Carlomagno and I. Grant, Sorrento, Italy, Paper 292, 1998.

[8]Naughton, J. W., and Brown, J. L., "Skin Friction Distribution near a Cylinder Mounted on a Flat Plate," AIAA Paper 97-1783, June 1997.

[9]Naughton, J. W., and Brown, J. L., "Uncertainty Analysis for Oil Film Interferometry Skin Friction Measurement Techniques," American Society of Mechanical Engineers, ASME Paper FEDSM97-3475, Vancouver, BC, Canada, June 1997.

[10]Naughton, J. W., and Brown, J. L., "Skin Friction Measurement in Complex Flows using Two-Image Thin-Oil-Film Interferometry," *8th International Symposium on Flow Visualization*, edited by G. M. Carlomagno and I. Grant, Sorrento, Italy, Paper 200, 1998.

[11]Naughton, J. W., and Brown, J. L., "Surface Interferometric Skin-Friction Measurement Technique," AIAA Paper 96-2183, June 1996.

[12]Brown, J. L., and Naughton, J. W., "The Thin Oil Film Equation," NASA TM 1999-208767, March 1999.

[13]Desse, J. M., "Three-Color Differential Interferometry," *Applied Optics*, Vol. 36, No. 28, 1997, pp. 7150–7156.

[14]Desse, J. M., "Recording and Processing of Interferograms by Spectral Characterisation of the Interferometric Setup," *Experiments in Fluids*, Vol. 23, 1997, pp. 265–271.

[15]Squire, H. B., and, Young, A. D., "The Calculation of Profile Drag of Airflow," Aeronautical Research Council, Repts. and Memoranda 1838, London, 1938.

[16]Schlichting, H., *Boundary-Layer Theory*, 6th ed., McGraw–Hill, New York, 1968, p. 128, 600.

R. P. Lucht
Associate Editor